Appl. Math. Mech. -Engl. Ed., **41**(9), 1431–1446 (2020)

APPLIED MATHEMATICS AND MECHANICS (ENGLISH EDITION)

https://doi.org/10.1007/s10483-020-2649-9

Electromagnetohydrodynamic flows and mass transport in curved rectangular microchannels*

Yongbo LIU, Yongjun JIAN†

School of Mathematical Science, Inner Mongolia University,
Hohhot 010021, China

(Received Feb. 3, 2020 / Revised Jun. 3, 2020)

Abstract Curved microchannels are often encountered in lab-on-chip systems because the effective axial channel lengths of such channels are often larger than those of straight microchannels for a given per unit chip length. In this paper, the effective diffusivity of a neutral solute in an oscillating electromagnetohydrodynamic (EMHD) flow through a curved rectangular microchannel is investigated theoretically. The flow is assumed as a creeping flow due to the extremely low Reynolds number in such microflow systems. Through the theoretical analysis, we find that the effective diffusivity primarily depends on five dimensionless parameters, i.e., the curvature ratio of the curved channel, the Schmidt number, the tidal displacement, the angular Reynolds number, and the dimensionless electric field strength parameter. Based on the obtained results, we can precisely control the mass transfer characteristics of the EMHD flow in a curved rectangular microchannel by appropriately altering the corresponding parameter values.

Key words electromagnetohydrodynamic (EMHD) flow, curved rectangular microchannel, mass transfer characteristic, effective diffusivity

Chinese Library Classification O357.1
2010 Mathematics Subject Classification 76W99, 74A60, 76A05

1 Introduction

Recently, many scholars have been interested in studying the transport phenomena in microchannels because of its various applications in chemistry[1–2], medicine[3–4], energy conversion[5], and mixing[6]. The fluid flow in microchannels can be driven by the pressure gradient[7–8], the electroosmosis force[9–16], and the Lorentz force[17–23]. Among these flows, the flow driven by the Lorentz force has the advantage of a larger flow rate. The Lorentz force is generated by the interaction of the externally applied orthogonal electric field and the magnetic field[17].

When a solute band is injected into a fluid flow, it is broaden by the hydrodynamic dispersion (HD) on account of the combined effects of nonuniformity in the fluid velocity and molecular

* Citation: LIU, Y. B. and JIAN, Y. J. Electromagnetohydrodynamic flows and mass transport in curved rectangular microchannels. *Applied Mathematics and Mechanics* (*English Edition*), **41**(9), 1431–1446 (2020) https://doi.org/10.1007/s10483-020-2649-9

† Corresponding author, E-mail: jianyj@imu.edu.cn

Project supported by the National Natural Science Foundation of China (No. 11772162) and the Natural Science Foundation of Inner Mongolia Autonomous Region of China (No. 2016MS0106)

diffusion. As a result, the solute dispersion is enhanced. This behavior may play an important role in the mass transfer characteristics of the flow. Therefore, the investigation of the HD in a channel flow is necessary. Many researchers have devoted to investigating the mass transfer problem owing to its wide range of applications in industrial processes and in drug delivery[24]. A lot of efforts have been put into the study of the enhanced mass transfer rates by periodic flows in particular. Aris[25] seems to be the first to reveal the enhanced longitudinal dispersion of the diffusing solute for periodic flows. Then, a general analytical theory for solute dispersion in oscillating flows of a Newtonian fluid was developed by Watson[26]. Joshi et al.[27] and Jaeger and Kurzweg[28] verified Watson's theory by conducting an experiment. The solute dispersion of a Jeffrey fluid between two parallel walls was studied by Manopoulos and Tsangaris[29]. They compared the effective diffusivity of a Jeffrey fluid with that of a Newtonian one, and demonstrated that the effective diffusivity of a Jeffrey fluid is larger than that of a Newtonian one.

Although all the aforementioned studies were investigated in macrochannels, the investigation of the HD in microchannels was also of importance[30–34]. Since the pressure-driven oscillatory flows are useful in increasing the mass transfer rate of the solute, experts speculated that the alternating current (AC)-driven electroosmotic flows (EOFs) in microchannels may be utilized to enhance the corresponding mass transfer rate. Huang and Lai[35] first investigated the enhanced mass transfer phenomenon in oscillatory EOFs through a parallel-plate microchannel. They demonstrated that under certain conditions, a larger mass flux can be induced by the oscillations of the externally applied electric fields. By using a cylindrical tube with a reactive wall, Ramon et al.[36] theoretically studied the mass transfer characteristics in an oscillatory EOF. Their results showed that the oscillatory EOF could be used for separation of species. Then, the corresponding model in a closed-ended cylindrical pore was given also by Ramon in their another work[37]. In addition, by employing a microtube, Li and Jian[38] investigated the HD in a periodic EOF of a Maxwell fluid. Another research team, led by Bautista, made important contributions to the investigations of the mass transfer characteristics in oscillatory EOFs. They showed that the mass transfer performance of such flows can be enhanced further by applying the asymmetric conditions of the wall zeta potentials[39], the slippage effect[40], the distinct periodic electric fields[41], and a Maxwell fluid[42].

Although the investigation of the solute dispersion by the EOF is very important, there still exist disadvantages. On one hand, when the electric double layers are very thin, the velocity profiles of the EOFs are almost uniform, leading to a weaker HD. On the other hand, the electromagnetohydrodynamic (EMHD) velocity is strongly nonuniform, which will lead to much stronger dispersion. Therefore, the EMHD flow may be chosen as an alternative flow for mass transfer. In spite of its important applications in mixing and separation problems, the HD in microchannels by EMHD flows was rarely studied by scholars[43–45]. Among these studies, the work given by Vargas et al.[45] was very important due to their consideration of the combined electroosmotic and magnetohydrodynamic effects.

In most of the investigations mentioned above, the channels involved were assumed as straight ones. However, curved microchannels may also have particular applications due to their advantage of avoiding entrance effects presenting in straight ducts. The EMHD flows in curved microchannels may be used to achieve micromixing processes. Most recently, Ortiz-Perez et al.[46] investigated the EMHD flow in an annular duct. Their results were useful in designing annular microfluidic devices. Then, Valenzuela-Delgado et al.[47] designed an experiment in an open annular channel to validate the corresponding mathematical model of the EMHD flow in such channels. However, although EMHD flows are important in the applications of mixing and separation, the mass transfer problem has not been analyzed yet. In addition, the study of the Maxwell fluid is also necessary due to its potential applications in mixing and separating of species[42].

Based on the above considerations, the theoretical analysis of the HD by EMHD flows of

a linearized Maxwell fluid through a curved rectangular microchannel is the objective of the present paper. The rest of the work is arranged as follows. In Section 2, under an externally applied periodic electric field and a stationary magnetic field, the equations of the flow velocity and the solute concentration are derived and their solutions are achieved. The variation trends of the effective diffusivity with its corresponding parameters are given in Section 3. Finally, we draw the conclusions in Section 4.

2 Problem formulation

In this paper, the HD in an oscillatory EMHD flow through a curved rectangular microchannel is considered. The geometry of the curved microchannel is shown in Fig. 1. We use a cylindrical coordinate system to analyze this problem, in which the r^*- and z^*-axes denote the radial direction and the vertical direction of the curved channel, respectively. The θ-axis denotes the flow direction. To drive the fluid flow in this channel, a periodic oscillating electric field with the amplitude E^* and a uniform magnetic field with the magnitude B^* are externally applied in the z^*-direction and in the r^*-direction, respectively. r_{i}^* and r_{o}^* are the inner radius and the outer radius of the curved channel, respectively, and $a^* = r_{\mathrm{o}}^* - r_{\mathrm{i}}^*$ represents the width of the rectangular cross section. In addition, b^* is the height of the rectangular cross section.

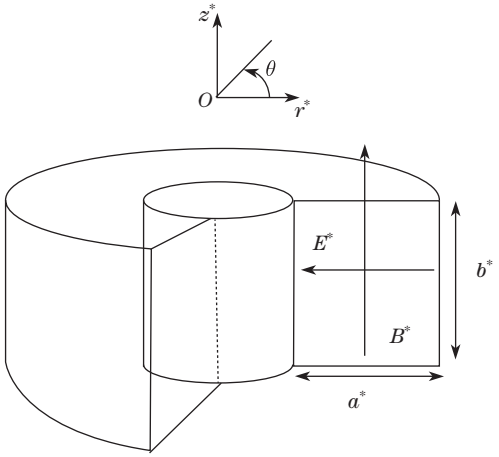

Fig. 1 Geometry of the curved microchannel

2.1 Analytical solution for the velocity field

The governing equations for the EMHD velocity distribution of an incompressible fluid are given as[20]

$$\nabla \cdot \boldsymbol{v} = 0, \tag{1}$$

$$\rho \boldsymbol{v} \cdot \nabla \boldsymbol{v} + \rho \frac{\partial \boldsymbol{v}}{\partial t} = -\nabla p + \nabla \cdot \boldsymbol{\tau} + \boldsymbol{J} \times \boldsymbol{B}, \tag{2}$$

where $\boldsymbol{v} = (v_{r^*}, v_{\theta^*}, v_{z^*})$ and $\boldsymbol{\tau}$ are the velocity vector and the stress tensor, and $\boldsymbol{J} = \sigma(\boldsymbol{E} + \boldsymbol{v} \times \boldsymbol{B})$ is the current density. ρ is the density of the fluid, p is the pressure, σ is the electrical conductivity of the fluid, and $\boldsymbol{E}$ is the periodic electric field with the magnitude E_0^*. Here, $E_0^* = \mathrm{Re}\{E^* \mathrm{e}^{-\mathrm{i}\omega^* t^*}\}$, in which Re denotes the real part of the function, E^* is the amplitude of the externally imposed electric field, i denotes the imaginary unit, ω^* denotes the oscillating frequency, and t^* is the time. $\boldsymbol{B}$ is the externally applied magnetic field with the magnitude B_0. The induced magnetic field is ignored since the magnetic Reynolds number Re_{m} (defined as the ratio of the advective term to the magnetic diffusive term in the equation of an induced magnetic field) is very small for a typical microchannel flow. Therefore, the velocity field and the induced

magnetic field are decoupled. The mathematical expression of the magnetic Reynolds number is $Re_{\mathrm{m}} = Ud\sigma\mu_{\mathrm{s}}$[46], where the magnitude of the characteristic velocity U is about $2\times10^{-3}\,\mathrm{m/s}$, the characteristic length d is about $500\,\mu\mathrm{m}$, and the magnetic diffusivity $\eta_{\mathrm{m}} = (\sigma\mu_{\mathrm{s}})^{-1}$ is about $10^{-2}\,\mathrm{m^2/s}$. As a result, the magnitude of the magnetic Reynolds number Re_{m} is about 10^{-4}, a very small parameter in such microchannel flows. For the flow assumed above, the component forms of the governing equations are expressed as follows[48]:

$$\frac{1}{r^*}\frac{\partial}{\partial r^*}(r^* v_{r^*}) + \frac{1}{r^*}\frac{\partial v_\theta}{\partial\theta} + \frac{\partial v_{z^*}}{\partial z^*} = 0, \tag{3}$$

$$\begin{aligned}&\rho\Big(v_{r^*}\frac{\partial v_{r^*}}{\partial r^*} + \frac{v_\theta}{r^*}\frac{\partial v_{r^*}}{\partial\theta} - \frac{v_\theta^2}{r^*} + v_{z^*}\frac{\partial v_{r^*}}{\partial z^*} + \frac{\partial v_{r^*}}{\partial t^*}\Big)\\ &= -\frac{\partial p}{\partial r^*} + \Big(\frac{1}{r^*}\frac{\partial}{\partial r^*}(r^*\tau_{r^*r^*}) + \frac{1}{r^*}\frac{\partial\tau_{r^*\theta}}{\partial\theta} + \frac{\partial\tau_{r^*z^*}}{\partial z^*} - \frac{\tau_{\theta\theta}}{r^*}\Big) - \sigma B_0^2 v_{r^*},\end{aligned} \tag{4}$$

$$\begin{aligned}&\rho\Big(v_{r^*}\frac{\partial v_\theta}{\partial r^*} + \frac{v_\theta}{r^*}\frac{\partial v_\theta}{\partial\theta} + \frac{v_{r^*}v_\theta}{r^*} + v_{z^*}\frac{\partial v_\theta}{\partial z^*} + \frac{\partial v_\theta}{\partial t^*}\Big)\\ &= -\frac{1}{r^*}\frac{\partial p}{\partial\theta} + \Big(\frac{1}{r^{*2}}\frac{\partial}{\partial r^*}(r^{*2}\tau_{r^*\theta}) + \frac{1}{r^*}\frac{\partial\tau_{\theta\theta}}{\partial\theta} + \frac{\partial\tau_{\theta z^*}}{\partial z^*} + \frac{\tau_{\theta r^*} - \tau_{r^*\theta}}{r^*}\Big) + \sigma E_0^* B_0 - \sigma B_0^2 v_\theta,\end{aligned} \tag{5}$$

$$\begin{aligned}&\rho\Big(v_{r^*}\frac{\partial v_{z^*}}{\partial r^*} + \frac{v_\theta}{r^*}\frac{\partial v_{z^*}}{\partial\theta} + v_{z^*}\frac{\partial v_{z^*}}{\partial z^*} + \frac{\partial v_{z^*}}{\partial t^*}\Big)\\ &= -\frac{\partial p}{\partial z^*} + \Big(\frac{1}{r^*}\frac{\partial}{\partial r^*}(r^*\tau_{r^*z^*}) + \frac{1}{r^*}\frac{\partial\tau_{\theta z^*}}{\partial\theta} + \frac{\partial\tau_{z^*z^*}}{\partial z^*}\Big).\end{aligned} \tag{6}$$

For the creeping flow assumed in this paper, the Reynolds number is very low so that the convective terms in Eqs. (4)–(6) can be neglected. In addition, determined by the externally applied electric field and the magnetic field, the Lorentz force is only along the θ-axis. This leads to the rectilinear distribution of the velocity field along the θ-axis[46], which means that $v_{r^*} = v_{z^*} = 0$. Substituting the assumption of $v_{r^*} = v_{z^*} = 0$ into Eq. (3), we obtain the following equation:

$$\frac{1}{r^*}\frac{\partial v_\theta}{\partial\theta} = 0. \tag{7}$$

Here, only the θ-momentum equation (5) needs to be solved. When the external pressure gradient is neglected, we obtain

$$\rho\frac{\partial v_\theta}{\partial t^*} = \Big(\frac{1}{r^{*2}}\frac{\partial}{\partial r^*}(r^{*2}\tau_{r^*\theta}) + \frac{1}{r^*}\frac{\partial\tau_{\theta\theta}}{\partial\theta} + \frac{\partial\tau_{\theta z^*}}{\partial z^*} + \frac{\tau_{\theta r^*} - \tau_{r^*\theta}}{r^*}\Big) + \sigma E_0^* B_0 - \sigma B_0^2 v_\theta. \tag{8}$$

The constitutive equation for the linearized Maxwell fluid is[49]

$$\boldsymbol{\tau} + t_{\mathrm{m}}\frac{\partial\boldsymbol{\tau}}{\partial t^*} = \eta(\nabla\boldsymbol{v} + (\nabla\boldsymbol{v})^{\mathrm{T}}), \tag{9}$$

where t_{m} is the relaxation time, and η is the viscosity of the fluid. In the cylindrical coordinate system, the corresponding components of the above constitutive equation are

$$\tau_{r^*\theta} + t_{\mathrm{m}}\frac{\partial\tau_{r^*\theta}}{\partial t^*} = \eta\Big(\frac{\partial v_\theta}{\partial r^*} - \frac{v_\theta}{r^*}\Big), \tag{10}$$

$$\tau_{\theta\theta} + t_{\mathrm{m}}\frac{\partial\tau_{\theta\theta}}{\partial t^*} = \eta\Big(\frac{2}{r^*}\frac{\partial v_\theta}{\partial\theta}\Big) = 0, \tag{11}$$

$$\tau_{\theta z^*} + t_{\mathrm{m}}\frac{\partial\tau_{\theta z^*}}{\partial t^*} = \eta\frac{\partial v_\theta}{\partial z^*}, \tag{12}$$

$$\tau_{\theta r^*} + t_{\mathrm{m}}\frac{\partial\tau_{\theta r^*}}{\partial t^*} = \eta\Big(\frac{\partial v_\theta}{\partial r^*} - \frac{v_\theta}{r^*}\Big). \tag{13}$$

Substituting Eqs. (10)–(13) into Eq. (8), the revised momentum equation can be rewritten as follows:

$$\begin{aligned}&\rho\Big(1+t_{\mathrm{m}}\frac{\partial}{\partial t^*}\Big)\frac{\partial v_\theta}{\partial t^*}\\&=\frac{1}{r^{*2}}\frac{\partial}{\partial r^*}\Big(r^{*2}\eta\frac{\partial v_\theta}{\partial r^*}-r^*\eta v_\theta\Big)+\frac{\partial}{\partial z^*}\Big(\eta\frac{\partial v_\theta}{\partial z^*}\Big)+\Big(1+t_{\mathrm{m}}\frac{\partial}{\partial t}\Big)(\sigma E_0^* B_0-\sigma B_0^2 v_\theta).\end{aligned}\tag{14}$$

No-slip boundary conditions are employed to Eq. (14), which are expressed as

$$(v_\theta)_{r^*=r_{\mathrm{i}}^*}=0,\quad (v_\theta)_{r^*=r_{\mathrm{o}}^*}=0,\quad (v_\theta)_{z^*=0}=0,\quad (v_\theta)_{z^*=b^*}=0.\tag{15}$$

In the present analysis, the velocity and the electric field are assumed harmonic with the same oscillating frequency ω^*. Thus, the velocity can be written as the complex form,

$$v_\theta=\mathrm{Re}\{U^*\mathrm{e}^{-\mathrm{i}\omega^* t^*}\},\tag{16}$$

where U^* is the amplitude of the axial velocity v_θ. Substituting Eq. (16) into Eq. (14) yields

$$\begin{aligned}&\eta\frac{\partial^2 U^*}{\partial z^{*2}}+\rho(\mathrm{i}\omega^*+\omega^{*2}t_{\mathrm{m}})U^*+\frac{\eta}{r^{*2}}\frac{\partial}{\partial r^*}\Big(r^{*2}\frac{\partial U^*}{\partial r^*}-r^*U^*\Big)\\&=-(1-\mathrm{i}\omega^* t_{\mathrm{m}})(\sigma E^* B_0-\sigma B_0^2 U^*).\end{aligned}\tag{17}$$

The following non-dimensional variables and parameters are introduced:

$$\begin{cases}u=\dfrac{U^*}{U},\quad r=\dfrac{r^*}{d},\quad z=\dfrac{z^*}{d},\quad a=\dfrac{a^*}{d},\quad b=\dfrac{b^*}{d},\quad S=\dfrac{E^* d}{U}\sqrt{\dfrac{\sigma}{\eta}},\\ Ha=B_0 d\sqrt{\dfrac{\sigma}{\eta}},\quad r_{\mathrm{i}}=\dfrac{r_{\mathrm{i}}^*}{d},\quad r_{\mathrm{o}}=\dfrac{r_{\mathrm{o}}^*}{d},\\ De=\omega^* t_{\mathrm{m}},\quad \alpha=\dfrac{a}{b},\quad Re_\omega=\dfrac{\rho\omega^* d^2}{\eta},\\ R_0^*=\dfrac{r_{\mathrm{i}}^*+r_{\mathrm{o}}^*}{2},\quad R_0=\dfrac{R_0^*}{d},\quad \delta=\dfrac{a}{2R_0},\end{cases}\tag{18}$$

where d is the hydraulic diameter of the microchannel, $U=\eta/(\rho d)$ is the characteristic velocity scale, Ha is the Hartmann number, S is the dimensionless electric field, and δ is the curvature ratio of the curved microchannel. De is the normalized relaxation time, α is the aspect ratio (width to height) of the rectangular cross section, Re_ω is the angular Reynolds number, and R_0 is the radius of the curvature. After substituting Eq. (18) into Eqs. (17) and (15), the modified momentum equation and its boundary conditions are normalized as

$$r^2\frac{\partial^2 u}{\partial r^2}+r\frac{\partial u}{\partial r}+r^2\frac{\partial^2 u}{\partial z^2}+((\mathrm{i}+De)(Re_\omega+\mathrm{i}Ha^2)r^2-1)u=(\mathrm{i}De-1)\cdot S\cdot Ha\cdot r^2,\tag{19}$$

$$(u)_{r=r_{\mathrm{i}}}=0,\quad (u)_{r=r_{\mathrm{o}}}=0,\quad (u)_{z=0}=0,\quad (u)_{z=b}=0.\tag{20}$$

The sinusoidal Fourier transformation is used to solve Eq. (19). Here, the corresponding Fourier transformation and its reverse relation are expressed as follows[48]:

$$F_s\{u(r,z)\}=v(r,n)=\frac{2}{b}\int_0^b u(r,z)\sin\Big(\frac{n\pi z}{b}\Big)\mathrm{d}z,\tag{21}$$

$$u(r,z)=F_s^{-1}\{v(r,n)\}=\sum_{n=1}^{\infty}v(r,n)\sin\Big(\frac{n\pi z}{b}\Big).\tag{22}$$

Applying the above transformation (21) into Eq. (19), we obtain

$$r^2\frac{\mathrm{d}^2v}{\mathrm{d}r^2}+r\frac{\mathrm{d}v}{\mathrm{d}r}-\Big((1-\mathrm{i}De)(Ha^2-\mathrm{i}Re_\omega)r^2+\frac{n^2\pi^2}{b^2}r^2+1\Big)v$$
$$=\frac{2}{n\pi}(\mathrm{i}De-1)(1-(-1)^n)\cdot S\cdot Ha\cdot r^2. \tag{23}$$

By introducing the modified Bessel function, the solution to the above equation is

$$v(r,n)=a_n(r)I_1(B_n\cdot r)+b_n(r)K_1(B_n\cdot r), \tag{24}$$

$$B_n=\sqrt{n^2\pi^2/b^2+(1-\mathrm{i}De)(Ha^2-\mathrm{i}Re_\omega)}, \tag{25}$$

$$\begin{cases} a_n(r)=\displaystyle\int_{r_\mathrm{i}}^{r}f(s)\mathrm{d}s+C_n,\\ b_n(r)=\displaystyle\int_{r_\mathrm{i}}^{r}-(I_1(B_n\cdot s)/K_1(B_n\cdot s))f(s)\mathrm{d}s+D_n, \end{cases} \tag{26}$$

$$f(r)=\Big(\frac{2}{n\pi}(1-\mathrm{i}De)S\cdot Ha\cdot r\cdot((-1)^n-1)\cdot K_1(B_n\cdot r)\Big)/(B_n\cdot r\cdot(K_1(B_n\cdot r)I_2(B_n\cdot r)$$
$$+I_1(B_n\cdot r)\cdot K_0(B_n\cdot r))+2K_1(B_n\cdot r)I_1(B_n\cdot r)), \tag{27}$$

$$C_n=-\frac{K_1(B_n\cdot r_\mathrm{i})}{I_1(B_n\cdot r_\mathrm{i})}D_n, \tag{28}$$

$$D_n=\Big(K_1(B_n\cdot r_\mathrm{o})I_1(B_n\cdot r_\mathrm{i})\int_{r_\mathrm{i}}^{r_\mathrm{o}}\frac{I_1(B_n\cdot s)}{K_1(B_n\cdot s)}f(s)\mathrm{d}s-I_1(B_n\cdot r_\mathrm{o})I_1(B_n\cdot r_\mathrm{i})\int_{r_\mathrm{i}}^{r_\mathrm{o}}f(s)\mathrm{d}s\Big)$$
$$\cdot(K_1(B_n\cdot r_\mathrm{o})I_1(B_n\cdot r_\mathrm{i})-K_1(B_n\cdot r_\mathrm{i})I_1(B_n\cdot r_\mathrm{o}))^{-1}. \tag{29}$$

Applying the reverse Fourier transformation (22) into Eq. (24), the analytical solution for the velocity distribution is finally obtained as

$$u(r,z)=\sum_{n=1}^{\infty}(a_n(r)I_1(B_n\cdot r)+b_n(r)K_1(B_n\cdot r))\sin(n\pi z/b). \tag{30}$$

2.2 Numerical solution for the solute concentration

The transport phenomenon in the present analysis will not be affected by the externally applied electric field owing to the assumption that the solute to be transported by the carrier liquid is electroneutral. In addition, for an infinitely dilute solute concentration assumed in this paper, the solute velocity is the same as the velocity of the carrier liquid. Therefore, the convection-diffusion equation for the concentration $C(r^*,\,\theta,\,z^*,\,t^*)$ can be given as

$$\frac{\partial C}{\partial t^*}+\frac{v_\theta}{r^*}\frac{\partial C}{\partial\theta}=\kappa\nabla^2C, \tag{31}$$

where κ is the constant diffusion coefficient. According to Watson's theory, the concentration $C(r^*,\,\theta,\,z^*,\,t^*)$ may be rewritten as[26]

$$C=-\gamma R_0^*\theta+\mathrm{Re}\{\gamma g^*(r^*,z^*)\mathrm{e}^{-\mathrm{i}\omega^*t^*}\}, \tag{32}$$

where g^* is the radial variation of the concentration field, and γ is the constant θ-axis concentration gradient, which is defined as

$$\frac{1}{R_0^*}\frac{\partial C}{\partial\theta}=-\gamma. \tag{33}$$

Substituting Eq. (32) into Eq. (31), we obtain the following equation:

$$\kappa\Big(\frac{\partial^2 g^*}{\partial r^{*2}}+\frac{1}{r^*}\frac{\partial g^*}{\partial r^*}+\frac{\partial^2 g^*}{\partial z^{*2}}\Big)+\mathrm{i}\omega^* g^*=-\frac{R_0^* U^*}{r^*}. \tag{34}$$

In addition, the following dimensionless parameters and quantities are defined:

$$Sc=\frac{\eta}{\rho\kappa},\quad Pe_\kappa=\frac{dU}{\kappa},\quad g=\frac{g^*}{d}, \tag{35}$$

where Sc is the Schmidt number, g is the dimensionless solute concentration, and Pe_κ is the diffusion Peclet number. Substituting Eqs. (18), (30), and (35) into Eq. (34) yields

$$\begin{aligned}&\frac{\partial^2 g}{\partial r^2}+\frac{1}{r}\frac{\partial g}{\partial r}+\frac{\partial^2 g}{\partial z^2}+\mathrm{i}Re_\omega Scg\\&=-\frac{R_0 Pe_\kappa}{r}\sum_{n=1}^{\infty}\left(a_n(r)I_1(B_n\cdot r)+b_n(r)K_1(B_n\cdot r)\right)\sin(n\pi z/b).\end{aligned} \tag{36}$$

The corresponding impermeable boundary conditions of Eq. (36) are[26]

$$\frac{\partial g}{\partial r}\Big|_{r=r_\mathrm{i}}=0,\quad \frac{\partial g}{\partial r}\Big|_{r=r_\mathrm{o}}=0,\quad \frac{\partial g}{\partial z}\Big|_{z=0}=0,\quad \frac{\partial g}{\partial z}\Big|_{z=b}=0. \tag{37}$$

The flux rate of the solute to be transported across any plane θ =constant is[26]

$$\begin{aligned}&\int_{r_\mathrm{i}^*}^{r_\mathrm{o}^*}\int_0^{b^*}\Big(v_\theta C-\kappa\frac{1}{R_0^*}\frac{\partial C}{\partial\theta}\Big)\mathrm{d}z^*\mathrm{d}r^*\\&=\int_{r_\mathrm{i}^*}^{r_\mathrm{o}^*}\int_0^{b^*}\Big(\frac{1}{2}(U^*\mathrm{e}^{-\mathrm{i}\omega^* t^*}+\overline{U}^*\mathrm{e}^{\mathrm{i}\omega^* t^*})\\&\quad\cdot\Big(-\gamma R_0^*\theta+\frac{1}{2}\gamma(g^*\mathrm{e}^{-\mathrm{i}\omega^* t^*}+\overline{g}^*\mathrm{e}^{\mathrm{i}\omega^* t^*})\Big)+\kappa\gamma\Big)\mathrm{d}z^*\mathrm{d}r^*,\end{aligned} \tag{38}$$

where the bars denote the complex conjugates. The time averaged rate of flux is

$$\int_{r_\mathrm{i}^*}^{r_\mathrm{o}^*}\int_0^{b^*}\Big(\kappa\gamma+\frac{1}{4}\gamma(U^*\overline{g}^*+\overline{U}^* g^*)\Big)\mathrm{d}z^*\mathrm{d}r^*. \tag{39}$$

In the absence of any flow, this would be $\kappa\gamma A$, and $A=a^*b^*$ is the area of the rectangular cross-section. The effective diffusivity in the oscillating flow is thus denoted as[29]

$$D_\mathrm{eff}^*=\kappa(1+D^*), \tag{40}$$

where

$$D^*=\frac{1}{4\kappa A}\int_{r_\mathrm{i}^*}^{r_\mathrm{o}^*}\int_0^{b^*}(U^*\overline{g}^*+\overline{U}^* g^*)\mathrm{d}z^*\mathrm{d}r^*. \tag{41}$$

Since the flow is an oscillatory flow, we may think that the effective diffusivity depends on the angular frequency. Now, we will introduce the concept of the tidal displacement Δz, which represents the average axial distance of a fluid particle during half an oscillating period. The mathematical expression of Δz is defined as[42]

$$\Delta z=\Big|\frac{1}{a^*b^*}\int_0^{b^*}\int_{r_\mathrm{i}^*}^{r_\mathrm{o}^*}\int_0^{\frac{\pi}{\omega^*}}v_\theta\mathrm{d}t^*\mathrm{d}r^*\mathrm{d}z^*\Big|. \tag{42}$$

Substituting Eqs. (16) and (18) into Eq. (42), we obtain the following expression:

$$\Delta z = \frac{2U}{\omega^* ab}\Big|\int_0^b \int_{r_\mathrm{i}}^{r_\mathrm{o}} u\mathrm{d}r\mathrm{d}z\Big|. \tag{43}$$

The dimensionless tidal displacement ΔZ is then given as

$$\Delta Z = \frac{\Delta z}{d} = \frac{2U}{\omega^* abd}\Big|\int_0^b \int_{r_\mathrm{i}}^{r_\mathrm{o}} u\mathrm{d}r\mathrm{d}z\Big|. \tag{44}$$

Equation (44) can be rewritten as follows:

$$U = \frac{\Delta Z \omega^* abd}{2\Big|\int_0^b \int_{r_\mathrm{i}}^{r_\mathrm{o}} u\mathrm{d}r\mathrm{d}z\Big|}. \tag{45}$$

Therefore, the Peclet number can be redefined as[42]

$$Pe_\omega = \frac{dU}{\kappa} = Re_\omega Sc \frac{\Delta Z ab}{2\Big|\int_0^b \int_{r_\mathrm{i}}^{r_\mathrm{o}} u\mathrm{d}r\mathrm{d}z\Big|}. \tag{46}$$

Finally, the non-dimensional effective diffusivity is obtained as[36]

$$D_\mathrm{eff} = \frac{D^*_\mathrm{eff}}{\kappa} = 1 + \frac{Pe_\omega}{4ab}\int_{r_\mathrm{i}}^{r_\mathrm{o}} \int_0^b (u\overline{g} + \overline{u}g)\mathrm{d}z\mathrm{d}r. \tag{47}$$

3 Results and discussion

Equations (36) and (17) are solved by the finite difference method, and we will give the detailed finite difference scheme in Appendix A[50]. In subsequent discussion, the corresponding parameters are set as the following values. Physically, $d = 500\,\mu\mathrm{m}$, $\sigma = 10^{-3} - 4\times10^3\,\mathrm{S/m}$, $\rho = 10^3\,\mathrm{kg/m^3}$, $\omega^* = 0{-}10^4\,\mathrm{rad/s}$, $\kappa = 10^{-9}{-}10^{-8}\,\mathrm{m^2/s}$, $t_\mathrm{m} = 10^{-3}{-}10^{-4}\,\mathrm{s}$, and $\eta = 10^{-3}\,\mathrm{kg/(ms)}$. When $t_\mathrm{m} \to 0$ (i.e., $De \to 0$), the Maxwell fluid in this paper approaches the classical Newtonian behavior[51]. The range of the imposed magnetic field is assumed as $O(B_0) = 0{-}5\,\mathrm{T}$. Therefore, the Hartmann number Ha changes from 0 to 5 by the definition in Eq. (18). For a typical microfluidic flow, the magnitude of the characteristic velocity is about $2\times10^3\,\mu\mathrm{m/s}$. When the externally imposed electrical field changes from $0\,\mathrm{V/m}$ to $0.02\,\mathrm{V/m}$, the variation range of S is 0–10. The domain of the diffusion Peclet number Pe_κ is $O(Pe_\kappa) = 100 - 1\,000$, since $Pe_\kappa = dU/\kappa$. As Munoz et al.[40] mentioned, the Schmidt number Sc varies from 100 to 2 000 according to different diffusion coefficient numbers. In addition, the dimensionless tidal displacement ΔZ changes from 0.5 to 2. In the present analysis, the range of the Deborah number De is 0.01 to 2π[52], and the range of the angular Reynolds number Re_ω is 1 to 3. Without special instruction, we let $r_\mathrm{i} = 1$ and $r_\mathrm{o} = 3$ in the following discussion.

In Fig. 2, we compare the present results with the existing theoretical results (Refs. [53] and [54]) and experimental results (Ref. [17]). Here, $Re_\omega = 0$ implies that the angular frequency $\omega^* = 0\,\mathrm{rad/s}$, which means that the externally imposed electric field is a constant number in this case. In addition, the curved rectangular microchannel tends to a straight one when $\delta \to 0$[48]. We find from Fig. 2 that the present results (when $De = 0$, $Re_\omega = 0$, and $\delta \to 0$) agree well with the existing data in a straight rectangular microchannel[17,52]. However, when $De > 0$ and $\delta = 0.5$, the velocity of the present model is smaller than that in a straight one.

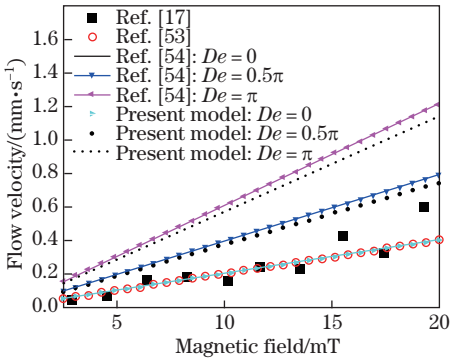

Fig. 2 Comparison of the present velocity with existing experimental and theoretical results (color online)

Figure 3 illustrates the influence of the dimensionless parameters, such as the dimensionless electric field strength S, the Deborah number De, and the angular Reynolds number Re_ω, on the solute concentration $g(r, z)$. The solute concentrations $g(r, z)$ increases with the growth of S and De. The reason behind these variation trends is that both the growth of S and of De can lead to the augmentation of the fluid velocity, and thus the convective mass transfer is enhanced ultimately. However, for a larger angular Reynolds number Re_ω, the fluid velocity is smaller due to the corresponding increase in the angular frequency ω^*. This variation trend was also found by Liu et al.[52] for an oscillating magnetohydrodynamic flow of a Maxwell fluid. Therefore, the solute concentrations $g(r, z)$ decreases with the increase in Re_ω.

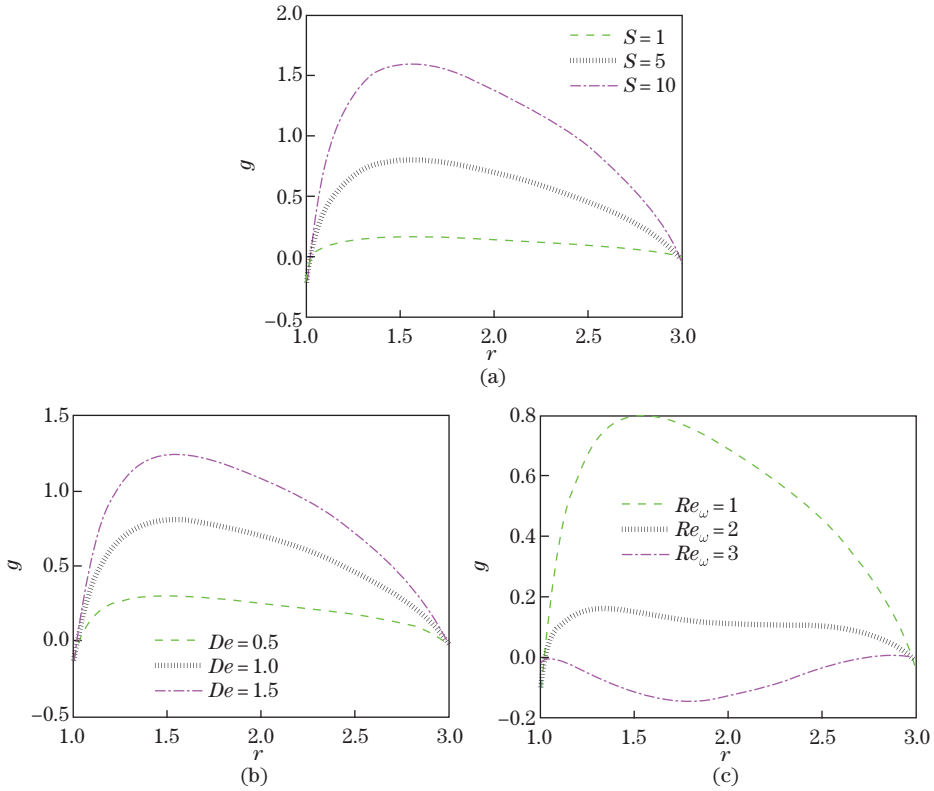

Fig. 3 Variations of the solute concentration $g(r, z)$ with r along the symmetry line ($z = b/2$) for different parameters when $Pe_\kappa = 1\,000$, $\alpha = 1$, $Ha = 1$, and $Sc = 1\,000$: (a) $Re_\omega = 1$ and $De = 1.0$; (b) $Re_\omega = 1$ and $S = 5$; (c) De =1.0 and $S = 5$ (color online)

Figure 4 delineates the variation trend of the solute concentration with r along the symmetry line ($z = b/2$) for different aspect ratios α. We can see from Fig. 4 that with the increase in α, the concentration $g(r, z)$ first increases and then decreases. The possible reason may be given as follows.

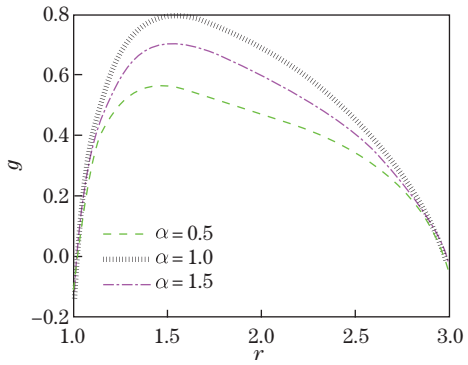

Fig. 4 Variations of the solute concentration $g(r, z)$ with r along the symmetry line ($z = b/2$) for different aspect ratios α when $Pe_\kappa = 1\,000$, $Ha = 1$, $Sc = 1\,000$, $Re_\omega = 1$, De =1.0, and $S = 5$ (color online)

The increase in α has two opposite effects on the variation trends of the solute concentration. First, the increase in α will lead to the decrease in the velocity, resulting in the decrease in the convective mass transfer and the decrease in the solute concentration. Second, in our discussion, we let $a = 2$, and thus the increase in α ($\alpha = a/b$) means the decrease in the rectangular cross section height b. Moreover, as b decreases, the solute will be more concentrated owing to the decreased region of the cross section. When α is small enough ($\alpha < 1$), the second effect is more important than the first one. Therefore, the solute concentration increases with α in this case. However, when the value of α is relatively large, a reversed variation trend is obtained.

Figure 5 shows the effect of the dimensionless Schmidt number Sc on the solute concentration $g(r, z)$ along the symmetry line ($z = b/2$). As is seen from Fig. 5, the solute concentration decreases with the increase in Sc. The reason may be that a larger Sc often signifies a smaller diffusion coefficient κ. This trend can be easily obtained from the definition of Sc given above. It is obvious that the decrease in the diffusion coefficient κ can lead to the decrease in the concentration values. Therefore, the solute concentration decreases with the dimensionless Schmidt number Sc.

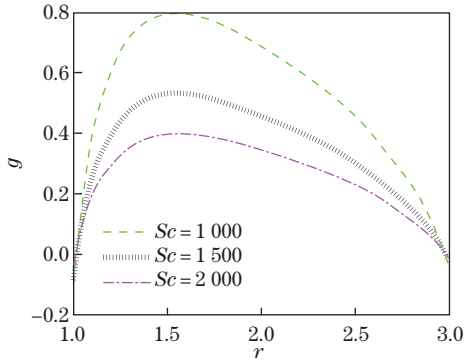

Fig. 5 Variations of the solute concentration $g(r, z)$ with r along the symmetry line ($z = b/2$) for different Schmidt numbers Sc when $Pe_\kappa = 1\,000$, $S = 5$, $Re_\omega = 1$, $De = 1.0$, $\alpha = 1$, and $Ha = 1$ (color online)

The effect of the diffusion Peclet number Pe_κ on the solute concentration profile is depicted in Fig. 6. It is obtained from Fig. 6 that the solute concentration increases with the growth of Pe_κ. The reason is that for larger values of Pe_κ considered here ($Pe_\kappa \geqslant 10$), the solute in the channel is mainly transported by the advection process instead of by diffusing. Therefore, the increase in Pe_κ implies the enhancement of the convection effect, leading to a larger solute concentration.

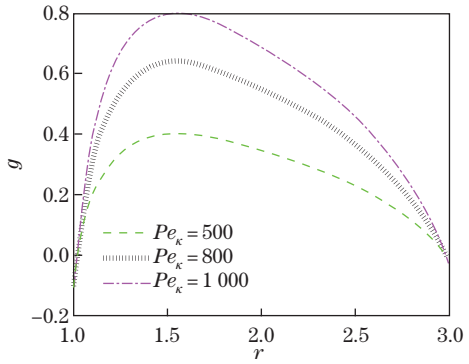

Fig. 6 Variations of the solute concentration $g(r, z)$ with r along the symmetry line ($z = b/2$) for different diffusion Peclet numbers Pe_κ when $S = 5$, $Re_\omega = 1$, De =1.0, $\alpha = 1$, $Ha = 1$, and $Sc = 1\,000$ (color online)

Figure 7 is devoted to studying the influence of the Schmidt number Sc, the tidal displacement ΔZ, the curvature ratio δ, the dimensionless electric field strength S, and the angular Reynolds number Re_ω on the graphs of the effective diffusivity D_{eff}. The first thing drawing our attention in Fig. 7 is that the effective diffusivity increases with the angular Reynolds number Re_ω. As the angular Reynolds number Re_ω increases, the velocity profiles become more non-uniform, resulting in the enhancement of the dispersion. In addition, we also find from Fig. 7 that D_{eff} increases with the increase in Sc, ΔZ, and S. First, with the increase in Sc and ΔZ, the angular frequency related Peclet number Pe_ω increases. As a result, the effective diffusivity is increased. Second, the velocity is amplified by increasing S. Hence, the increase trend of D_{eff} with S is reasonable. In addition, Fig. 7(c) shows that the effective diffusivity D_{eff} decreases with the increase in the curvature ratio δ, which is more obvious for larger Re_ω. This is because the increase in the curvature ratio will decrease the velocity gradient and eventually lower the mass transport rate. These results may be useful in controlling the mass transfer characteristics in an EMHD flow through a curved rectangular microchannel.

In Fig. 8, we depict the variation trends of the effective diffusivity with the angular Reynolds number for two different species. Here, glucose and ethanol are chosen as two different solutes to be transported. The mass diffusion coefficients in water for glucose and ethanol are 0.690×10^{-9} and 1.200×10^{-9}, respectively. Accordingly, the corresponding Schmidt numbers are 1 271.01 and 730.833, respectively. Obviously, the diffusivity of glucose in water is lower than that of ethanol when the fluid is at rest. However, when the angular Reynolds number is larger, i.e., $Re_\omega > 0.4$, the effective diffusivity of glucose could exceed that of ethanol. This phenomenon can be used to separate different species in a fluid.

4 Conclusions

The mass transport characteristics of an oscillatory EMHD flow of a Maxwell fluid through a curved rectangular microchannel are analyzed in detail. After theoretical derivation and

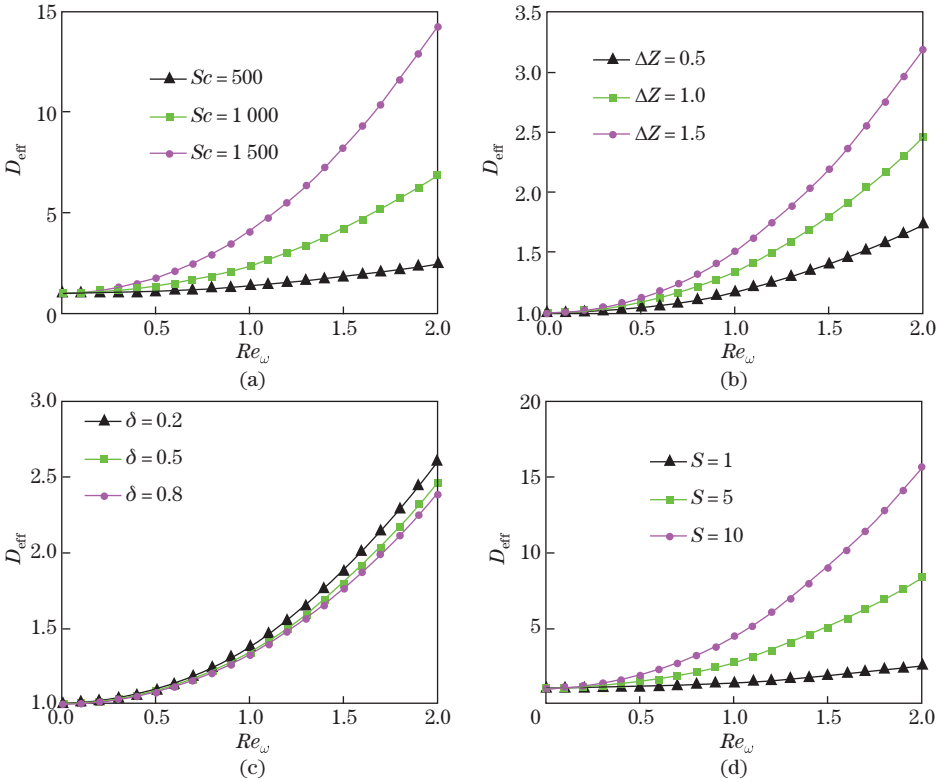

Fig. 7 Variations of the dimensionless effective diffusivity for different parameters (a) $\Delta Z = 1$, $\delta = 0.5$, and $S = 1$; (b) $Sc = 500$, $\delta = 0.5$, and $S = 1$; (c) $Sc = 500$, $\Delta Z = 1$, and $S = 1$; (d) $\Delta Z = 1$, $\delta = 0.5$, and $Sc = 500$ when $De = 1.0$ and $Ha = 1$ (color online)

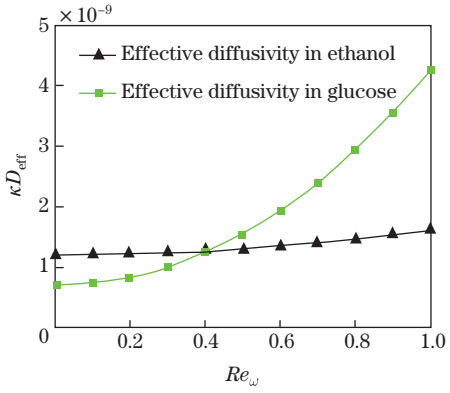

Fig. 8 Variations of the effective diffusivity of two different species with the angular Reynolds number for glucose and ethanol diffusers in water as the carrier. The values of the corresponding parameters involved are $Ha = 1$, $\Delta Z = 1$, $\delta = 0.5$, $S = 1$, and $De = 1.0$ (color online)

graphical analysis, the following interesting conclusions are obtained. Our results demonstrate that the effective diffusivity $D_{\rm eff}$ is decreased by the curvature ratio δ, which means that the curved rectangular microchannel can be used to slow the mixing down. However, the effective diffusivity $D_{\rm eff}$ shows increasing trends with the increase in the Schmidt number Sc, the tidal displacement ΔZ, the dimensionless electric field strength S, and the angular Reynolds number

Re_ω. In addition, we also find that under certain parameter ranges, the effective diffusivity of slow diffusers (such as glucose) in an oscillating EHMD flow could exceed that of fast diffusers (such as ethanol). These conclusions could be used as a guidance in designing micro-devices for mixing or separation of species.

References

[1] STONE, H. A., STROOCK, A. D., and AJDARI, A. Engineering flows in small devices: microfluidics toward a lab-on-a-chip. *Annual Review of Fluid Mechanics*, **36**(36), 381–411 (2004)

[2] SARKAR, S. and GANGULY, S. Characterization of electromagnetohydrodynamic transport of power law fluids in microchannel. *Journal of Non-Newtonian Fluid Mechanics*, **250**, 18–30 (2017)

[3] KLEINSTREUER, C., JIE, L., and JUNEMO, K. Microfluidics of nano-drug delivery. *International Journal of Heat and Mass Transfer*, **51**(23), 5590–5597 (2008)

[4] KHAN, I. U., SERRA, C. A., ANTON, N., and VANDAMMEA, T. Microfluidics: a focus on improved cancer targeted drug delivery systems. *Journal of Controlled Release*, **172**(3), 1065–1074 (2013)

[5] MANSOURI, A., BHATTACHARJEE, S., and KOSTIUK, L. High-power electro kinetic energy conversion in a glass microchannel array. *Lab on a Chip*, **12**(20), 4033–4036 (2012)

[6] LIU, Y. Z., KIM, B. J., and SUNG, H. J. Two-fluid mixing in a microchannel. *International Journal of Heat and Fluid Flow*, **25**(6), 986–995 (2004)

[7] WEILIN, Q., MALA, G. M., and LI, D. Q. Pressure-driven water flows in trapezoidal silicon microchannels. *International Journal of Heat and Mass Transfer*, **43**(3), 353–364 (2000)

[8] CHANDA, S., SINHA, S., and DAS, S. Streaming potential and electroviscous effects in soft nanochannels: towards designing more efficient nanofluidic electrochemomechanical energy converters. *Soft Matter*, **10**(38), 7558–7568 (2014)

[9] DAS, S. and CHAKRABORTY, S. Analytical solutions for velocity, temperature and concentration distribution in electroosmotic microchannel flows of a non-Newtonian bio-fluid. *Analytica Chimica Acta*, **559**(1), 15–24 (2006)

[10] TSAO, H. K. Electroosmotic flow through an annulus. *Journal of Colloid and Interface Science*, **225**(1), 247–250 (2000)

[11] TAN, Z., QI, H. T., and JIANG, X. Y. Electroosmotic flow of Eyring fluid in slit microchannel with slip boundary condition. *Applied Mathematics and Mechanics* (*English Edition*), **35**(6), 689–696 (2014) https://doi.org/10.1007/s10483-014-1822-6

[12] WANG, C. Y., LIU, Y. H., and CHANG, C. C. Analytical solution of electro-osmotic flow in a semicircular microchannel. *Physics of Fluids*, **20**(6), 063105 (2008)

[13] DING, Z. D., JIAN, Y. J., and YANG, L. G. Time periodic electroosmotic flow of micropolar fluids through microparallel channel. *Applied Mathematics and Mechanics* (*English Edition*), **37**(6), 769–786 (2016) https://doi.org/10.1007/s10483-016-2081-6

[14] WANG, X., CHEN, B., and WU, J. A semianalytical solution of periodical electro-osmosis in a rectangular microchannel. *Physics of Fluids*, **19**(12), 127101 (2007)

[15] QI, C. and NG, C. O. Rotating electroosmotic flow of viscoplastic material between two parallel plates. *Colloids and Surfaces A*: *Physicochemical and Engineering Aspects*, **513**, 355–366 (2017)

[16] QI, C. and NG, C. O. Electroosmotic flow of a power-law fluid in a slit microchannel with gradually varying channel height and wall potential. *European Journal of Mechanics-B/Fluids*, **52**, 160–168 (2015)

[17] LEMOFF, A. V. and LEE, A. P. An AC magnetohydrodynamic micropump. *Sensors and Actuators B*: *Chemical*, **63**(3), 178–185 (2000)

[18] SHEIKHOLESLAMI, M. and BHATTI, M. M. Forced convection of nanofluid in presence of constant magnetic field considering shape effects of nanoparticles. *International Journal of Heat and Mass Transfer*, **111**, 1039–1049 (2017)

[19] DANIEL, Y. S., AZIZ, Z. A., ISMAIL, Z., and SALAH, F. Slip effects on electrical unsteady MHD natural convection flow of nanofluid over a permeable shrinking sheet with thermal radiation. *Engineering Letters*, **26**(1), 107–116 (2018)

[20] JANG, J. and LEE, S. S. Theoretical and experimental study of MHD (magnetohydrodynamic) micropump. *Sensors and Actuators A*: *Physical*, **80**(1), 84–89 (2000)

[21] CHAKRABORTY, S. and PAUL, D. Microchannel flow control through a combined electromagnetohydrodynamic transport. *Journal of Physics D*: *Applied Physics*, **39**(24), 5364–5371 (2006)

[22] DAS, S., MITRA, S. K., and CHAKRABORTY, S. Ring stains in the presence of electromagnetohydrodynamic interactions. *Physical Review E*, **86**(5), 056317 (2012)

[23] ESCANDON, J., SANTIAGO, F., BAUTISTA, O., and MENDEZ, F. Hydrodynamics and thermal analysis of a mixed electromagnetohydrodynamic-pressure driven flow for Phan-Thien-Tanner fluids in a microchannel. *International Journal of Thermal Sciences*, **86**, 246–257 (2014)

[24] WEIGL, B. H., BARDELL, R. L., and CABRERA, C. R. Lab-on-a-chip for drug development. *Advanced Drug Delivery Reviews*, **55**(3), 349–377 (2003)

[25] ARIS, R. On the dispersion of a solute in pulsating flow through a tube. *Proceedings of the Royal Society of London*, *Series A*, *Mathematical and Physical Sciences*, **259**(1298), 370–376 (1960)

[26] WATSON, E. J. Diffusion in oscillatory pipe flow. *Journal of Fluid Mechanics*, **133**, 233–244 (1983)

[27] JOSHI, C. H., KAMM, R. D., DRAZEN, J. M., and SLUTSKY, A. S. An experimental study of gas exchange in laminar oscillatory flow. *Journal of Fluid Mechanics*, **133**, 245–254 (2006)

[28] JAEGER, M. J. and KURZWEG, U. H. Determination of the longitudinal dispersion coefficient in flows subjected to high-frequency oscillations. *Physics of Fluids*, **26**(6), 1380–1382 (1983)

[29] MANOPOULOS, C. and TSANGARIS, S. Enhanced diffusion for oscillatory viscoelastic flow. *Physica Scripta*, **89**(8), 085206 (2014)

[30] ZHOU, Q. and NG, C. O. Electro-osmotic dispersion in a circular tube with slip-stick striped wall. *Fluid Dynamics Research*, **47**(1), 015502 (2014)

[31] NG, C. O. and CHEN, B. Dispersion in electro-osmotic flow through a slit channel with axial step changes of zeta potential. *Journal of Fluids Engineering*, **135**(10), 101203 (2013)

[32] NG, C. O. and ZHOU, Q. Dispersion due to electroosmotic flow in a circular microchannel with slowly varying wall potential and hydrodynamic slippage. *Physics of Fluids*, **24**(11), 112002 (2012)

[33] JIE, S., NG, C. O., and ADRIAN, W. K. Dispersion in oscillatory electro-osmotic flow through a parallel-plate channel with kinetic sportive exchange at walls. *Journal of Hydrodynamics*, **26**(3), 363–373 (2014)

[34] ARCOS, J. C., MÉNDEZ, F., BAUTISTA, E. G., and BAUTISTA, O. Dispersion coefficient in an electro-osmotic flow of a viscoelastic fluid through a microchannel with a slowly varying wall zeta potential. *Journal of Fluid Mechanics*, **839**, 348–386 (2018)

[35] HUANG, H. F. and LAI, C. L. Enhancement of mass transport and separation of species by oscillatory electroosmotic flows. *Proceedings of the Royal Society A*: *Mathematical*, *Physical and Engineering Sciences*, **462**(2071), 2017–2038 (2006)

[36] RAMON, G., AGNON, Y., and DOSORETZ, C. Solute dispersion in oscillating electro-osmotic flow with boundary mass exchange. *Microfluidics and Nanofluidics*, **10**(1), 97–106 (2011)

[37] RAMON, G. Z. Solute transport under oscillating electro-osmotic flow in a closed-ended cylindrical pore. *Journal of Engineering Mathematics*, **110**(1), 195–205 (2018)

[38] LI, H. C. and JIAN, Y. J. Dispersion for periodic electro-osmotic flow of Maxwell fluid through a microtube. *International Journal of Heat Mass Transfer*, **115**, 703–713 (2017)

[39] MEDINA, I., TOLEDO, M., MÉNDEZ, F., and BAUTISTA, O. Pulsatile electroosmotic flow in a microchannel with asymmetric wall zeta potentials and its effect on mass transport enhancement and mixing. *Chemical Engineering Science*, **184**, 259–272 (2018)

[40] MUÑOZ, J., ARCOS, J., BAUTISTA, O., and MÉNDEZ, F. Slippage effect on the dispersion coefficient of a passive solute in a pulsatile electro-osmotic flow in a microcapillary. *Physical Review Fluids*, **3**, 084503 (2018)

[41] TEODORO, C., BAUTISTA, O., and MÉNDEZ, F. Mass transport and separation of species in an oscillating electro-osmotic flow caused by distinct periodic electric fields. *Physica Scripta*, **94**(11), 115012 (2019)

[42] PERALTA, M., ARCOS, J., MÉNDEZ, F., and BAUTISTA, O. Mass transfer through a concentric-annulus microchannel driven by an oscillatory electroosmotic flow of a Maxwell fluid. *Journal of Non-Newtonian Fluid Mechanics*, **279**, 104281 (2020)

[43] ZHAO, J., ZHENG, L., ZHANG, X., and LIU, F. Convection heat and mass transfer of fractional MHD Maxwell fluid in a porous medium with Soret and Dufour effects. *International Journal of Heat Mass Transfer*, **103**, 203–210 (2016)

[44] SRINIVAS, S. and KOTHANDAPANI, M. The influence of heat and mass transfer on MHD peristaltic flow through a porous space with compliant walls. *Applied Mathematics and Computation*, **213**(1), 197–208 (2009)

[45] VARGAS, C., BAUTISTA, O., ARCOS, J., and MENDEZ, F. Hydrodynamic dispersion in a combined magnetohydrodynamic-electroosmotic-driven flow through a microchannel with slowly varying wall zeta potentials. *Physics of Fluids*, **29**(9), 0922002 (2017)

[46] ORTIZ-PEREZ, A. S., GARCIA-ANGEL, V., ACUNA-RAMIREZ, A., VARGAS-OSUNA, L., PEREZ-BARRERA, E. J., and CUEVAS, S. Magnetohydrodynamic flow with slippage in an annular duct for microfluidic applications. *Microfluidics and Nanofluidics*, **21**(8), 138 (2017)

[47] VALENZUELA-DELGADO, M., FLORES-FUENTES, W., RIVAS-LOPEZ, M., SERGIYENKO, O., LINDNER, L., HERNANDEZ-BALBUENA, D., and RODRIGUEZ-QUINONEZ, J. C. Electrolyte magnetohydrodynamic flow sensing in an open annular channel — a vision system for validation of the mathematical model. *Sensors*, **18**(6), 1683 (2018)

[48] NOROUZI, M., VAMERZANI, B. Z., DAVOODI, M., BIGLARI, N., and SHAHMARDAN, M. M. An exact analytical solution for creeping Dean flow of Bingham plastics through curved rectangular ducts. *Rheologica Acta*, **54**(5), 391–402 (2015)

[49] DEHARO, M. L., DELRIO, J. A., and WHITAKER, S. Flow of Maxwell fluids in porous media. *Transport in Porous Media*, **25**(2), 167–192 (1996)

[50] SAUER. T. *Numerical Analysis*, 2nd ed., Pearson Education Inc., New York, 399–401 (2012)

[51] BANDOPADHYAY, A. and CHAKRABORTY, S. Giant augmentations in electro-hydro-dynamic energy conversion efficiencies of nanofluidic devices using viscoelastic fluids. *Applied Physics Letters*, **101**(4), 043905 (2012)

[52] LIU, Y. P., JIAN, Y. J., LIU, Q. S., and LI, F. Q. Alternating current magnetohydrodynamic electroosmotic flow of Maxwell fluids between two micro-parallel plates. *Journal of Molecular Liquids*, **211**, 784–791 (2015)

[53] RIVERO, M. and CUEVAS, S. Analysis of the slip condition in magnetohydrodynamic (MHD) micropumps. *Sensors and Actuators B*: *Chemical*, **166**, 884–892 (2012)

[54] ZHAO, G. P., JIAN, Y. J., CHANG, L., and BUREN, M. D. L. Magnetohydrodynamic flow of generalized Maxwell fluids in a rectangular micropump under an AC electric field. *Journal of Magnetism and Magnetic Materials*, **387**, 111–117 (2015)

Appendix A

We will solve Eq. (36) on a rectangle $[r_\mathrm{i}, r_\mathrm{o}]\times[0, b]$ in the plane, with the boundary conditions given in Eq. (37). To obtain the numerical solution to Eq. (36), a rectangular mesh of points is given first in Fig. A1. In the horizontal direction and vertical direction, we use $M = m - 1$ steps and $N = n-1$ steps, respectively. As a result, the mesh sizes in the r- and z-directions are $h = (r_\mathrm{o} - r_\mathrm{i})/M$ and $k = (b - 0)/N$, respectively. First, Eq. (36) is rewritten as follows:

$$\frac{\partial^2 g}{\partial r^2} + \frac{1}{r}\frac{\partial g}{\partial r} + \frac{\partial^2 g}{\partial z^2} + \mathrm{i}Re_\omega Scg = -\frac{R_0 Pe_\kappa}{r}u, \tag{A1}$$

where $u(r,z)=\sum\limits_{n=1}^{\infty}(a_n(r)I_1(B_n\cdot r)+b_n(r)K_1(B_n\cdot r))\sin(n\pi z/b)$ represents the obtained velocity. By using the centered-difference formula, Eq. (A1) has the following finite difference form[50]:

$$\frac{g(r-h,\ z)-2g(r,\ z)+g(r+h,\ z)}{h^2}+\frac{1}{r}\frac{g(r+h,\ z)-g(r,\ z)}{h}+\frac{g(r,\ z-k)-2g(r,\ z)+g(r,\ z+k)}{k^2}$$
$$+\mathrm{i}Re_\omega Scg(r,\ z)+O(h^2)+O(h)+O(k^2)=-\frac{R_0Pe_\kappa}{r}u(r,\ z). \tag{A2}$$

In terms of the approximate solution, $w_{\bar{i},\ \bar{j}}\approx g(r_{\bar{i}},\ z_{\bar{j}})$ can be written as

$$\frac{w_{\bar{i}-1,\ \bar{j}}-2w_{\bar{i},\ \bar{j}}+w_{\bar{i}+1,\ \bar{j}}}{h^2}+\frac{1}{r_{\bar{i}}}\frac{w_{\bar{i}+1,\ \bar{j}}-w_{\bar{i},\ \bar{j}}}{h}+\frac{w_{\bar{i},\ \bar{j}-1}-2w_{\bar{i},\ \bar{j}}+w_{\bar{i},\ \bar{j}+1}}{k^2}+\mathrm{i}Re_\omega Scw_{\bar{i},\ \bar{j}}$$
$$=-\frac{R_0Pe_\kappa}{r_{\bar{i}}}u_{\bar{i},\ \bar{j}}, \tag{A3}$$

where $r_{\bar{i}}=r_{\mathrm{i}}+(\bar{i}-1)h$, and $z_{\bar{j}}=(\bar{j}-1)k$ for $1\leqslant\bar{i}\leqslant m$ and $1\leqslant\bar{j}\leqslant n$.

Each boundary point needs an equation as well, from the boundary conditions expressed in Eq. (37), we have the following equations:

Bottom: $\dfrac{w_{\bar{i},\bar{j}+1}-w_{\bar{i},\bar{j}}}{k}=0\quad$ for $\quad\bar{j}=1,\quad 1\leqslant\bar{i}\leqslant m.$

Top side: $\dfrac{w_{\bar{i},\bar{j}}-w_{\bar{i},\bar{j}-1}}{k}=0\quad$ for $\quad\bar{j}=n,\quad 1\leqslant\bar{i}\leqslant m.$

Left side: $\dfrac{w_{\bar{i}+1,\bar{j}}-w_{\bar{i},\bar{j}}}{h}=0\quad$ for $\quad\bar{i}=1,\quad 2\leqslant\bar{j}\leqslant n-1.$

Right side: $\dfrac{w_{\bar{i},\bar{j}}-w_{\bar{i}-1,\bar{j}}}{h}=0\quad$ for $\quad\bar{i}=m,\quad 2\leqslant\bar{j}\leqslant n-1.$

The above problem is solved by using Newton's method.

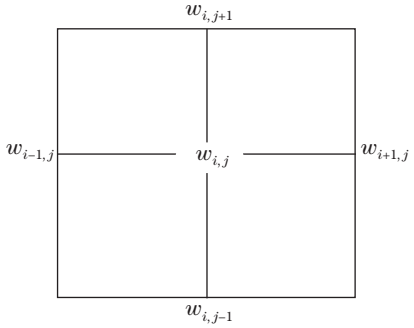

Fig. A1 Computational mesh